CALIBRATION OF RADAR BASED RE-ENTRY PREDICTIONS

S. Lemmens[(1)], B. Bastida Virgili[(1)], T. Flohrer[(2)], F. Gini[(3)], H. Krag[(2)], C. Steiger[(4)]

[(1)] IMS Space Consultancy, Space Debris Office, Robert-Bosch-Straße 5, 64293 Darmstadt, Germany, Email:Stijn.Lemmens@esa.int.
[(2)] European Space Agency, Space Debris Office, Robert-Bosch-Straße 5, 64293 Darmstadt, Germany.
[(3)] European Space Agency, Navigation Support Office, Robert-Bosch-Straße 5, 64293 Darmstadt, Germany.
[(4)] European Space Agency, Solar and Planetary Missions Division, Robert-Bosch-Straße 5, 64293 Darmstadt, Germany.

ABSTRACT

The availability of GPS observations via the telemetry during GOCE's (Gravity Field and Steady-State Ocean Circulation Explorer) entire re-entry campaign enabled the generation of high quality orbit products which can be used as input to re-entry predictions. These high precision orbits can be used as reference to assess the quality of orbits generated from other sources. Here we verify the accuracy of orbits based on radar tracking data, obtained by dedicated observations with the Tracking & Imaging Radar system from the Fraunhofer High Frequency Physics and Radar Techniques institute, with respect to the a post-processed GPS based reference orbit. This leads to time-depended quantification of the orbit determination uncertainties on the re-entry predictions. Furthermore, the ballistic coefficient determined by the orbit determination and its time dependent evolution can be used to a priori estimate the attitude behaviour of GOCE, which can be compared to the telemetry. The attitude behaviour can be analysed by the use of inverse synthetic aperture radar (ISAR) images, also obtained by dedicated observation by TIRA. The effect of adding this knowledge on the attitude evolution to the re-entry predictions is evaluated.

1. INTRODUCTION

The re-entry of ESA's Gravity Field and Steady-State Ocean Circulation Explorer (GOCE) satellite in November 2013 was an exceptional one. The satellite remained fully operational until its last orbit, sending a final batch of housekeeping telemetry at an altitude of about 105km. GOCE's re-entry was followed on international level as part of a yearly Inter-Agency Space Debris Coordination Committee (IADC) re-entry test campaign. The campaign was opened on October 21 2013 when GOCE reached fuel depletion at an altitude of about 225km. From that date on, GOCE was bound to undergo a natural decay which lead to an uncontrolled re-entry on Nov. 11th 2013 at 00:16UTC, when the atmospheric interface at 80km altitude was crossed. Until this point in time, the spacecraft was still assumed to be fully functional, apart from its orbit control capacity. The last successful station pass over the Troll station in Antarctica with fully nominal reception of telemetry occurred around 1h before the actual re-entry. To the best of our knowledge, there has never been contact to a spacecraft in such a low altitude undergoing an uncontrolled re-entry. This yields a rich dataset, which contains GPS based orbital positions as well as attitude states derived from the on-board attitude control system that has been collected by the spacecraft and downloaded up to the last pass down to an altitude of about 128km [1].

Independent of ESA, during the re-entry phase the satellite laser ranging (SLR) community has tracked GOCE at least twice through the International Laser Ranging Service (ILRS). Many other sensors have followed GOCE as well, and provided ESA with their results, e.g. through orbital elements received from USSTRATCOM and observations acquired by the Fraunhofer institute for High Frequency Physics and Radar Techniques (FHR), within the frame of the IADC's 2013-1 re-entry test campaign. The combination of collected "in-situ" data with external observations enables a cross-calibration of the different data sources, and the focus of this paper is on the orbital data derived from FHR's Tracking & Imaging Radar (TIRA) data [2].

2. RADAR BASED ORB IT DETERMINATION

During the last three weeks before GOCE's re-entry on the 11th of November 2013, 12 dedicated passes of the spacecraft were observed by FHR's TIRA in Wachtberg, Germany. During seven of these passes, Inverse Synthetic Aperture Radar (ISAR) images of the spacecraft were created. Moreover, continuous GPS telemetry is available until the last data batch was downlinked on the 10th of November at 17:15 UTC. Both sources can be used by independent methods for the purpose of orbit determination. An overview of the radar passes where GOCE was tracked by TIRA is given in Tab. 1.

Proc. '5th International GOCE User Workshop', Paris, France 25–28 November 2014 (ESA SP-728, March 2015)

Table 1: Meta-information on the passes of GOCE as observed by TIRA.

Pass	Start epoch (UTC)	End epoch (UTC)	Min. Range [km]	Max. elevation [deg]	ISAR imaging
1	2013/10/22T07:17:06	2013/10/22T07:22:28	404.1	34.3	Yes
2	2013/10/22T18:49:49	2013/10/22T18:56:02	402.4	33.4	No
3	2013/10/23T07:01:55	2013/10/23T07:07:49	642.4	18.8	No
4	2013/10/29T18:19:42	2013/10/29T18:25:49	309.2	44.6	Yes
5	2013/10/30T07:58:24	2013/10/30T08:03:37	440.9	28.5	No
6	2013/10/31T07:37:27	2013/10/31T07:43:47	221.3	81.0	Yes
7	2013/11/07T07:44:20	2013/11/07T07:49:54	228.4	56.1	No
8	2013/11/08T07:14:26	2013/11/08T07:19:32	451.6	22.1	No
9	2013/11/08T18:38:50	2013/11/08T18:44:14	203.4	62.7	Yes
10	2013/11/09T08:08:58	2013/11/09T08:13:44	568.5	15.5	Yes
11	2013/11/09T18:05:00	2013/11/09T18:09:47	537.5	16.2	Yes
12	2013/11/10T07:32:04	2013/11/10T07:37:02	189.8	55.5	Yes

For all 12 radar passes listed above, it was attempted to derive an orbit state, as well as to derive an improved orbit by combining multiple passes. Towards this goal, ESA's Orbit Determination via Improved Normal Equations (ODIN) software was used. ODIN implements modules for radar tracking data processing, initial orbit determination, and full orbit determination by batch least-square fitting, Levenberg-Marquardt optimisation, rank reductions and other techniques [3].
Based on the Root-Mean-Square (RMS) values of the fitted orbit w.r.t. the range, azimuth and elevation data from the passes, it is possible to assess the quality of the fitted orbital state. For the TIRA sensor, RMS values in the order of decametres for range and centi-degrees for azimuth and elevation for two or three passes over the course of less than two days are considered as good enough for re-entry predictions. These obtained RMS values can go up to hectometres in range and deci-degrees in elevation and azimuth for four or more passes over two or more days. Based on the residuals between fitted orbit and observations, outliers can be discarded and the orbit determination process repeated. The final decision on the acceptance of an orbit for re-entry predictions remains a decisions to be taken by a human operator. From the 12 passes in Tab. 1, 15 orbits are derived for re-entry predictions and listed with their main characteristics in Tab. 2.

Example residuals of a such a good fit w.r.t. the observation data, as provided by fit no. 13, are given in Figs. 1, 2, and 3. Here the perceived range and azimuth biases, in respectively Fig. 1 and Fig. 2, are compensated for by a better fit during the other two passes. The divergences visible in the elevation data in Fig. 3 are typical for low elevation observations.

On the other side of the spectrum, an example for a bad fit is taken from fit no. 3, where the azimuth residuals in Fig. 4 display highly non-linear behaviour. The orbit state was selected for re-entry predictions based on its low RMS, which were due to the fact that most of the measurement points were already rejected by the orbit determination process converging to a wrong result.

The orbit determination process does not only estimate the orbit state, but the station position and time biases, and the object drag coefficient (Cd) as well. The estimated drag coefficient, given in Tab 2, can be scaled with an aerodynamic reference area of $1.035m^2$ and reference mass of 1002 kg to obtain the estimated ballistic parameter for the spacecraft. As can be seen in Tab. 2 and Fig. 5, the estimated Cd values show a significant variation and dependency on the observation epoch. We will refer separately to the fitted states with fit epoch in October and the ones in November. A linear regression model is estimated with the state epoch as explanatory variable and the fitted drag coefficient as response variable. The standard deviation of the residuals of the model is 0.124.

3. RADAR BASED ATTITUDE DETERMINATION

When deriving an orbital state from radar tracking data, no assumptions are made on the attitude of the object under scrutiny. Instead, the effects of changes in the attitude state during observation and between passes are absorbed by the estimation of the drag coefficient.

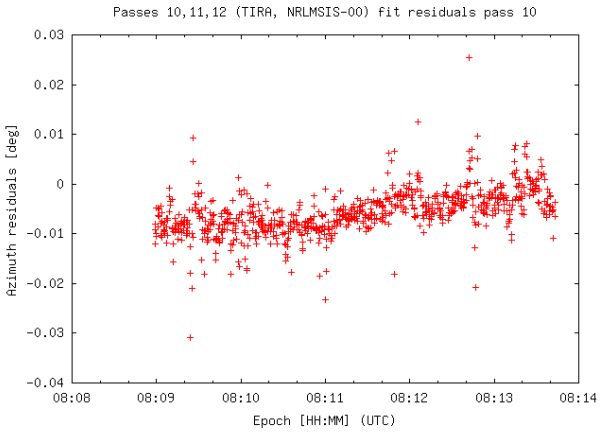

Figure 1: Good fit (no. 13) range residuals.

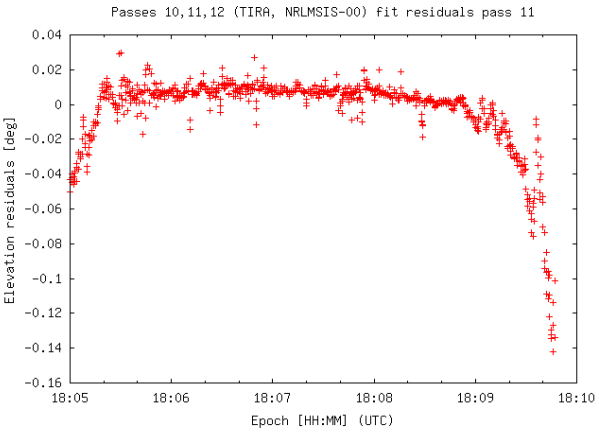

Figure 3: Good fit (no. 13) elevation residuals.

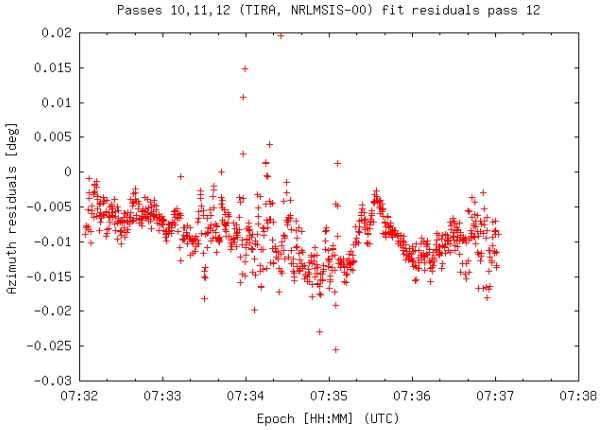

Figure 2: Good fit (no. 13) azimuth residuals.

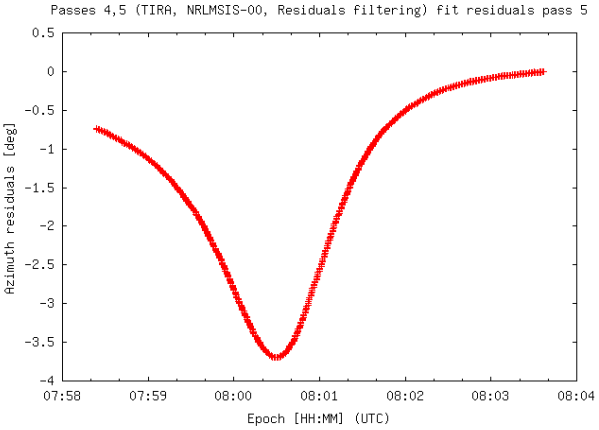

Figure 4: Bad fit (no. 3) azimuth residuals.

Table 2: Meta-information on the fitted radar observation states.

Fit number	Orbit Determination Epoch (UTC)	No. Passes [-]	Fitted Cd [-]	Range RMS [km]	Azimuth RMS [deg]	Elevation RMS [deg]	Ref. Range RMS [km]
1	2013/10/22-07:30:00	1	3.385	0.1257E-01	0.4290E-02	0.8290E-02	0.146640
2	2013/10/23-07:15:00	1,2,3	3.679	0.4315E-01	0.1169E-01	0.1824E-01	0.074246
3	2013/10/30-08:15:00	4,5	3.370	0.2846E-01	0.1984E-01	0.3444E-01	18.30148
4	2013/10/31-08:00:00	4,5,6	3.624	0.5088E-01	0.1772E-01	0.2556E-01	0.161752
5	2013/11/08-08:15:44	7,8	3.920	0.2012E-01	0.1677E-01	0.1586E-01	0.109213
6	2013/11/08-18:40:44	7,8,9	3.774	0.3100E-01	0.1503E-01	0.1856E-01	0.121194
7	2013/11/09-08:10:44	7,8,9,10	3.659	0.8932E+00	0.4179E+00	0.3844E+00	3.720242
8	2013/11/09-08:10:44	8,9,10	3.556	0.3270E-01	0.1083E-01	0.2089E-01	0.141724
9	2013/11/09-18:07:44	8,9,10	3.676	0.8766E+00	0.2463E-01	0.1478E+00	1.838436
10	2013/11/09-18:07:44	9,10,11	3.761	0.4064E-01	0.1102E-01	0.2435E-01	0.237662
11	2013/11/09-18:07:44	9,10,11	3.761	0.4063E-01	0.1102E-01	0.2435E-01	0.237661
12	2013/11/10-07:35:44	9,10,11,12	3.824	0.7512E+00	0.3225E-01	0.1158E+00	1.483740
13	2013/11/10-07:35:44	10,11,12	3.911	0.5193E-01	0.9270E-02	0.2697E-01	0.195948
14	2013/11/10-07:35:44	11,12	3.642	0.1619E-01	0.9965E-02	0.2231E-01	0.148577
15	2013/11/10-07:35:44	10,12	3.842	0.1982E-01	0.2725E-01	0.2242E-01	0.271460

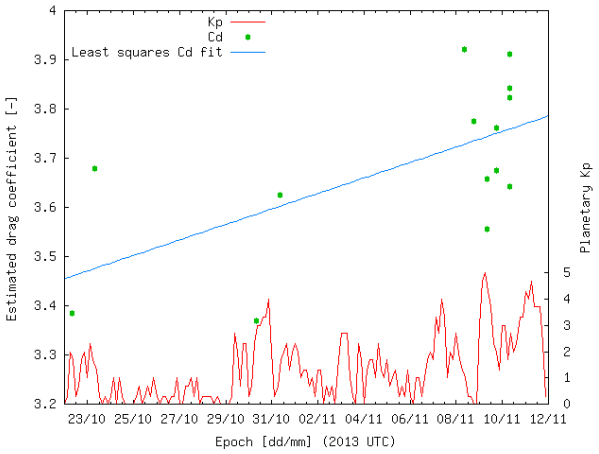

Figure 5: Fitted and estimated drag coefficient from TIRA tracking in comparison to the solar weather as presented by the planetary Kp index.

As seen in Fig.5, it can be tempting to draw the conclusion that there is a linear trend in the Cd data which should be taken into account for re-entry predictions, but it is import to understand, whether this behaviour is due to an attitude law or modelling deficiencies. For GOCE, the attitude in case of a controlled, i.e. fine pointing mode (FPM) until re-entry, or uncontrolled, i.e. unstable spin or aerodynamically stabilised depending on the altitude where FPM is lost, has been analysed with a six degrees of freedom propagator [1].

Inverse synthetic aperture radars (ISAR) are valuable instruments for assessing the state of a large object in low Earth orbit. The imaging capabilities of these radars, such as TIRA, can reach a sufficient quality for their products to be used during launch support or contingency operations, e.g. determining the structural integrity, or analysing the dynamic behaviour of an object. However, the direct interpretation of ISAR images can be a demanding task due to the nature of the range-Doppler space in which these images are produced. A tool called MOWA (Models on Orbit with an Attitude) has been developed by ESA's Space Debris Office to generate radar mappings of a target in orbit. These mappings are a 3D-model based simulation of how an ideal ISAR image would be generated by a ground based radar under given conditions, and can be used to support a data interpretation process [4].

Seven out of the twelve radar pass observations included the generation of ISAR images. From these observations, it is possible to derive the attitude of GOCE. In hindsight, none of the uncontrolled attitude scenarios anticipated for GOCE happened, and all seven observations were made with GOCE in FPM. In this mode, the symmetry axis of the spacecraft is almost parallel with the velocity direction of the orbit. The symmetry axis can move in the plane perpendicular to the orbit plane, which contains the orbit velocity vector, i.e. a yaw motion. This attitude motion is controlled by magneto-torquers and allows for an offset of ±6 degrees.

With the observations made during FPM mode, the resolution of the attitude solution based on ISAR images can be analysed. A fit score approach has been developed for automated attitude matching on ISAR images which is used to derive the likelihood of different scenarios [5]. In Fig. 7, an example overview is given, analysing five scenarios where different varying yaw configurations are compared. However, pure small yaw motion under the given observation condition for GOCE results in a rotational difference perpendicular to the range-Doppler space used for ISAR images and is thus mostly unresolvable. Hence, the attitude resolution down to degrees in Euler angles which has been achieved for other satellites could not be reproduced for GOCE in the observed FPM. This implied that the dependence of the drag coefficient on the attitude could not be discarded based on radar observations alone.

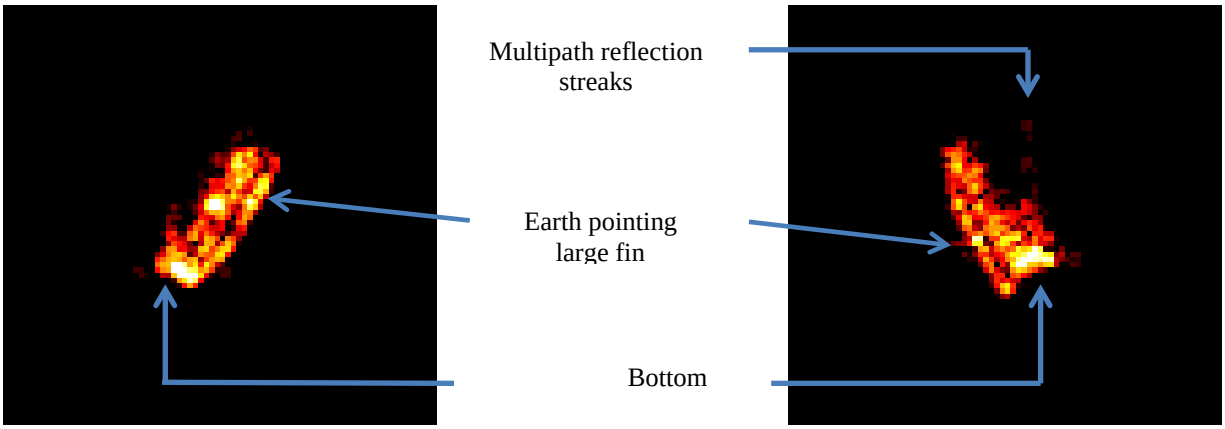

Figure 6: ISAR images of GOCE by FHR TIRA.

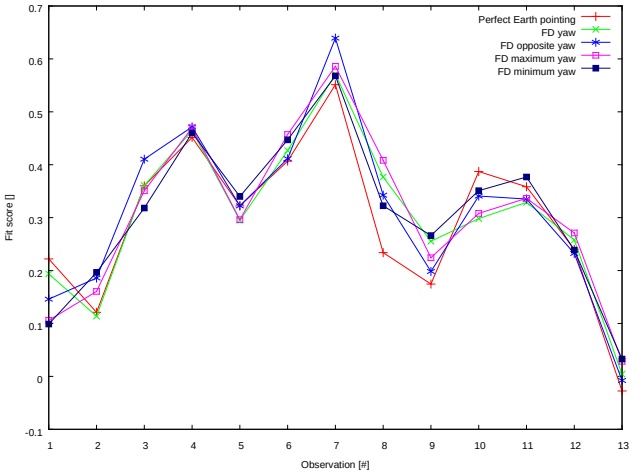

Figure 7: Comparison of the fit scores for the pass no. 1 for attitude scenarios within the . ±6 degrees yaw constraint.

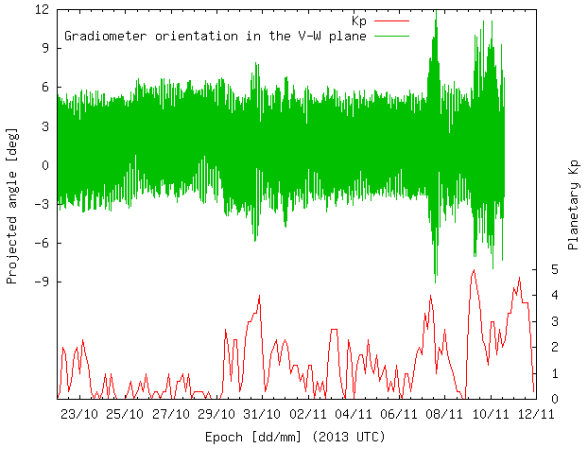

Figure 8: GOCE yaw attitude in comparison to the solar weather as presented by the planetary Kp index.

Taking into account the actual attitude of GOCE, a clear correlation between the yaw motion and space weather events can be established. In Fig. 8, the yaw angle is compared to the planetary Kp index, which captures the geomagnetic activity in near Earth space. Three major X-class flares occurred during re-entry in November and one in October, which are visible as peaks in the Kp index and yaw angle. As such, the variation and offset between the estimated drag coefficient values from the radar are likely to stem from un-modelled disturbances of the atmosphere.

4. GPS BASED ORBIT DETERMINATION

The GPS data available for the re-entry phase has been processed with the ESA/ESOC NAPEOS software. A sequence of programs has been defined to achieve Precise Orbit Determination (POD) as is available for the science phase. The sequence is implemented to process the data and estimate the daily orbital arcs. At an extremely low altitude between 230 km and 130 km, i.e. altitudes at which the GPS data were successfully downlinked, the main non-gravitational perturbation was the atmospheric drag. During this orbital decay an increment of a factor of 100 in the aerodynamic acceleration profile was observed. In order to limit the mismodelling of the non-gravitational forces, e.g. radiation pressure and aerodynamic effects, the newly developed software Aerodynamics and Radiation Pressure Analysis (ARPA) has been adopted to compute the forces acting on GOCE [6]. A full overview of the orbit determination process is given in [7].

The post-fit RMS of the undifferenced carrier phase residuals shows values between 6 and 14 mm for the first 16 daily arcs, which then increase with the decrement of the orbit altitude, reaching a level of about 80 mm on the last available day, where the altitude is about 130 km. The estimated empirical accelerations show higher values at the end of the observed re-entry, as the altitude of the satellite decreases and the aerodynamic forces get higher. From the ARPA modelling a reduction of these empirical accelerations is observed, with an average decrement of about 20% in the along-track and 40% in the cross-track directions. This GPS derived orbit will be referred to as the reference orbit.

5. RADAR DERIVED ORBIT QUALITY

Selecting as reference the precise orbits independently derived from the GPS observations, we are in position to analyse the accuracy of the 15 radar tracking derived orbits. Tab. 2 lists the RMS values w.r.t. the observations for the fitted orbits as well as w.r.t. a reference orbit in the ‘Ref. Range’ column. For the latter, the difference in position between the radar derived orbit and the reference orbit is computed. Furthermore, also the RMS is computed for the difference values during the passes used for the orbit determination.

In general, the range RMS for the observations and for the reference orbit w.r.t. the fitted states correlates well. An example of a good fit, reusing the previous example fit no. 13, spanning one day and three observation passes is given in Fig 9. The difference between the radar derived orbit and the reference obit are computed in the radial, transverse and normal direction of an orbit system associated with the reference orbit. The accuracy of the radar derived orbit is within the expected accuracy defined by the observation accuracy, i.e. hectometres radial, kilometres along track, and decametres cross-track. An example of a bad fit, reusing the previous example fit no. 3, is given in Fig. 10.

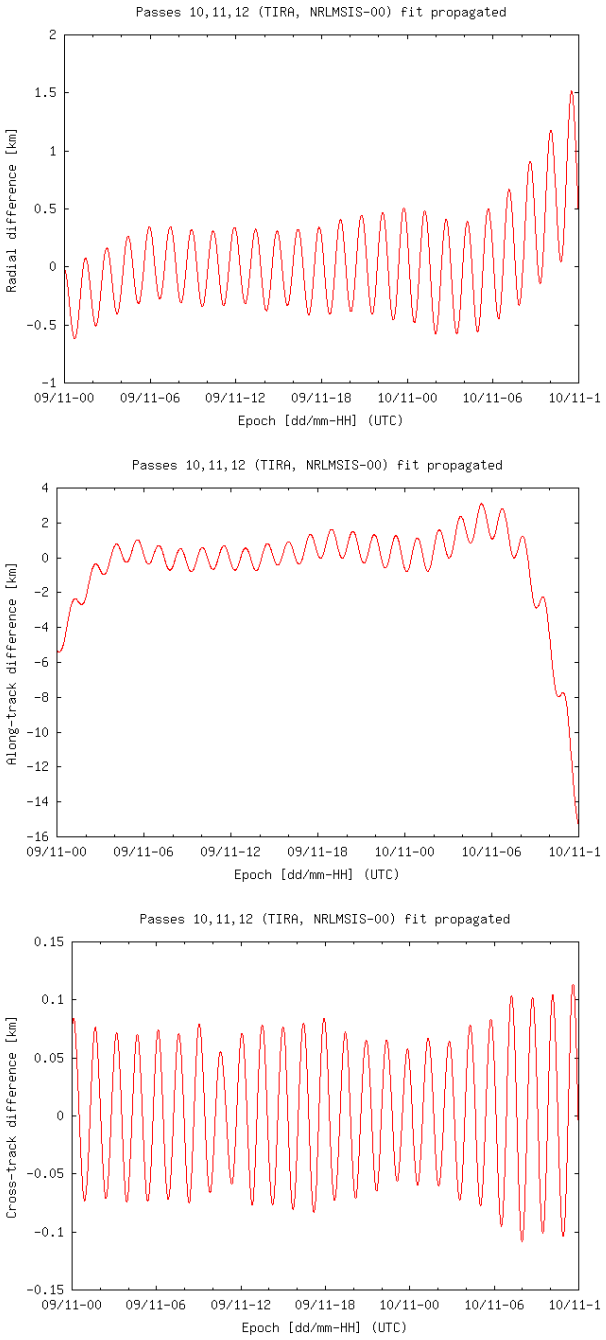

Figure 9: Differences in an orbit reference frame for the radar derived orbit (fit no.13) w.r.t. the reference orbit.

The tracking data used for this fit was acquired from two passes, and, due to stringent pre-filtering and tracking geometry, is too coarse to capture the information on the eccentricity of the orbit. This does not only imply an error on the radial difference between radar derived and reference orbits, but also a timing error which translates into an error in the along-track position as visible in Fig. 11. We conclude, however, that radar tracking can provide comparable information to meet re-entry prediction needs as would the illusory availability of on-board GPS. The acquired

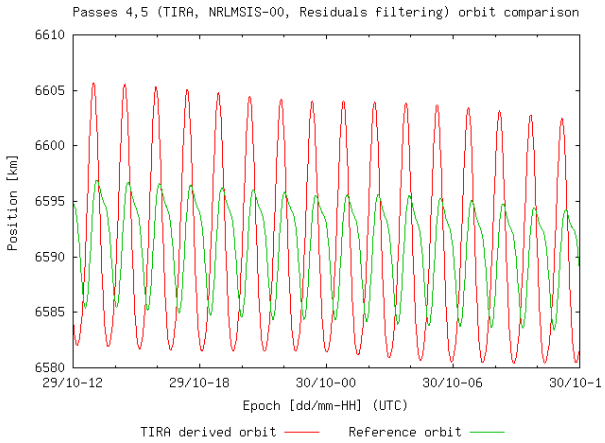

Figure 10: Range difference for the radar derived orbit (fit no.3) w.r.t. the reference orbit.

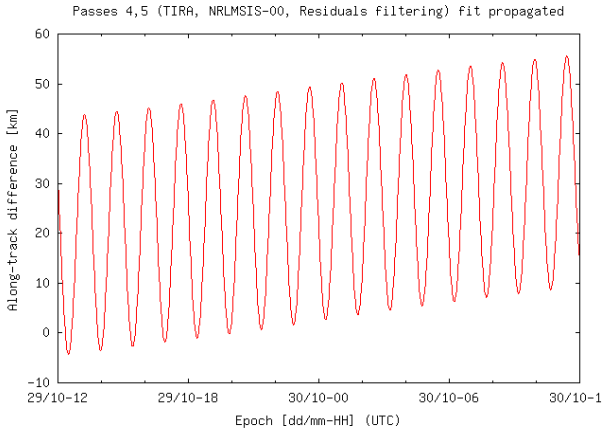

Figure 11: Difference in an orbit reference frame for the radar derived orbit (fit no.3) w.r.t. the reference orbit.

passes need to ensure a proper estimation of the eccentricity. To achieve this from a single site radar, one needs observation batches 12-14h apart, covering different local pass directions. This is not without challenges for the convergence of the orbit determination during the late re-entry phases and may conflict with the assumption of a consistent attitude motion over that time span.

6. RE-ENTRY PREDICTIONS

The 15 fitted orbital states of GOCE can serve as input states to the process of re-entry predictions. Under re-entry predictions we understand the computational methods required to predict the orbit evolution of an indestructible object in space expected to impact on ground due to loss of altitude as a result of orbit perturbations. In the relevant literature, an uncertainty value of 20% of the remaining lifetime is considered as a conservative estimate to be added to the re-entry epoch in order to define the re-entry window [8]. This uncertainty is mainly driven by the uncertainties on the drag coefficient, the orbital state, and the atmosphere and its interaction with the space weather environment.

To verify or constrain this 20% rule of thumb for GOCE and using radar observations only, a statistical sample is defined. For every pass which was used to derive a state given in Tab.2, a state from the fitted orbit during the pass is selected. The Cd value associated to this state is chosen by random sampling of a Gaussian distribution with its epoch dependent mean defined by the presented least square fit and the variance equal to the variance on the residuals of the same least squares fit. This variation of the Cd value captures the uncertainty on the attitude state of the object when treated as an unknown. To further capture the uncertainties on the space weather and specifically the occurrences of geomagnetic storms, a statistical Kp prediction model has been developed and integrated within the available orbit propagator for re-entry predictions. The appearance of geo-magnetic storms, defined as a point in time where the three hourly Kp index exceeds 5, as a function of the phase within a solar cycle, has been analysed by modelling the period between two geo-magnetic storms as a Poisson process. Historical frequency counts are made of the three hourly Kp indices in winnowed storm and inter-storm periods. Simplifying the situation further, the Kp indices within both periods, grouped by their phase in the solar cycle, are treated as independent. As such, a probability distribution function (PDF) can be derived from the frequency counts. These PDFs, together with the gap model between storms, can then be used to generate a statistical cycle given the phase values, which in turn can be derived from the average mean sunspot number, measured or predicted. The details of this procedure can be found in [9]. In total, 26 distinct Kp sequences have been generated for the GOCE re-entry phase. For the F10.7, the a posteriori measured data has been used.

Given the process defined above, 234 orbit states with drag coefficient and Kp environment were generated with starting date in October 2013 and 1144 with starting date in November 2013. All these states are propagated forward by a numerical propagator until an equatorial perigee height of 128 km is reached. This height corresponds to the end of the reference orbit as derived from GPS observations. At this point in the orbit, the epoch of the propagated orbit is compared to the final epoch of the reference orbit, i.e. the reference epoch. In Fig 12 and 13, the propagated epochs for all 15 states from Tab. 2 with their estimated epochs are displayed. All are within the 20 per cent boundary window. In Fig. 14 and 15, the propagated epochs for all sampled states as described above are presented. Again, for the states of October 2013 all are within the 20% window. The epoch distribution is a symmetric one with a bias towards earlier re-entry epochs. This implies that the Cd value is already overestimated, but the spread w.r.t. the average prediction epoch can be reduced to 10% of the remaining lifetime. For the November 2013 states, where the maximum remaining lifetime amounts to 4 days, the qualitative behaviour is similar. All obtained predictions are within the 20% window defined by the four day lifetime, whereas more than 90% are within the 20% window defined by the last available state, 10 hours before the reference epoch. It should be pointed out that this data set contains states spread out between 10 hours and four days before the reference epoch, hence, the 20% uncertainty window can shrink in this case as well to 10% and still contain all epochs.

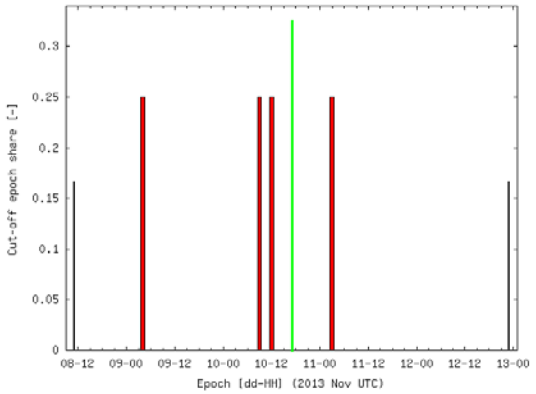

Figure 12: Predictions for fitted states from October. The black bars are boundaries of the 20% interval taking the last available state. the green bar is the ref. epoch.

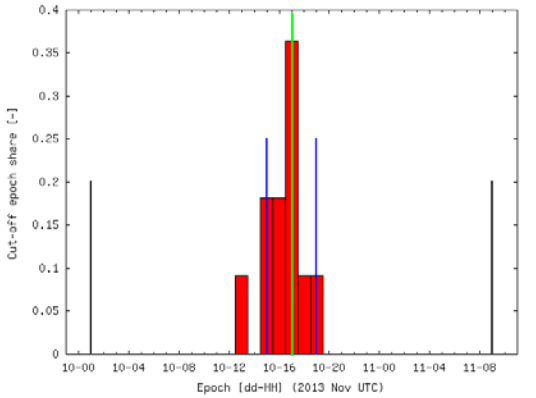

Figure 13: Predictions for fitted states from November. The black/blue bars are the 20% interval boundaries taking the first/last available state, the green bar is the ref. epoch.

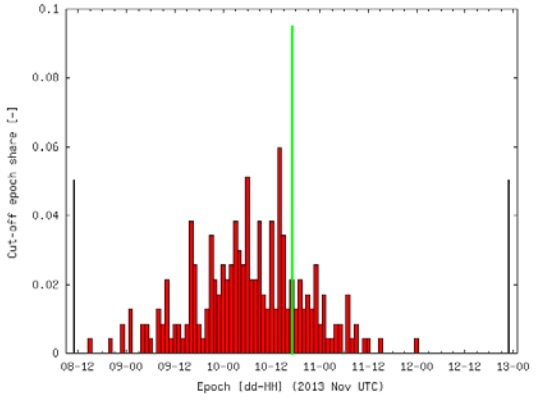

Figure 14: Predictions for sampled states from October. The black bars are the 20% interval boundaries taking

the last available state, the green bar is the ref. epoch.

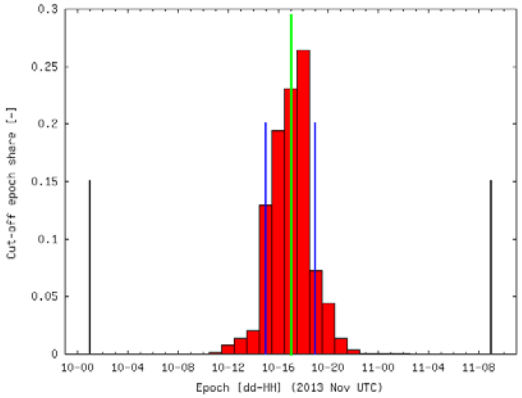

Figure 15: Predictions for sampled states from November. The black/blue bars are the 20% interval boundaries taking the first/last available state, the green bar is the ref. epoch.

7. CONCLUSIONS

The accuracy of re-entry predictions based solely on radar tracking and imaging has been investigated by using GOCE as an example. To this end, orbits derived from at most twice a day radar tracks have been compared to a GPS derived reference orbit, down to an orbit altitude of 128km at the equator. To account for perturbations in the atmosphere model, a Gaussian error was applied to the drag coefficient estimated from the radar passes as well as using a statistical model for the planetary Kp values during the re-entry phase. Under these assumptions, a conservative approach generally expects an uncertainty on the re-entry epoch on the order of 20% of the remaining orbital lifetime at the prediction epoch. For GOCE, it was significantly less than this, with an average error on the order of 10% of the remaining lifetime.

Radar tracking can provide information comparable to on-board GPS solutions, when the goal is to reduce the uncertainties currently associated with re-entry predictions. However, a proper observation strategy has to be in place, i.e. acquired passes need to ensure a proper estimation of the eccentricity, which results in at least 12-14h covering with observation batches and different local pass directions for a single site. Otherwise the error is absorbed in the drag coefficient. This can be challenging depending on the object's orbit. Moreover, the observation geometry allowing for a decent orbit sampling does not have to correspond to the best geometry for observing attitudes.

GOCE's attitude and orbit behaviour leaves room for more exploitation. One large uncertainty remains the state of the atmosphere during the re-entry phase. In further activities, it will be investigated to which extent the lessons learned from the GOCE re-entry predictions can be extended to other bodies which could be aerodynamically stabilised, e.g. rocket bodies.

8. REFERENCES

1. B. Bastida Virgili, T. Flohrer, S. Lemmens, et al (2014). GOCE Re-entry Campaign. *Proceedings of the fifth international GOCE user workshop*, ESA Publications Division, European Space Agency, Noordwijk, The Netherlands.

2. Mehrholz D. (1993). Space Object Observation with Radar. *Advances in Space Research*, Vol. 13, No. 8, pp. 833-842.

3. Alarcón J.R., Klinkrad H., Cuesta J. & Martinez F.M. (2005). Independent Orbit Determination for collision Avoidance. *Proceedings of the Fourth European conference on Space Debris*, ESA SP-587, ESA Publications Division, European Space Agency, Noordwijk, The Netherlands.

4. S. Lemmens, H. Krag, (2013). Radar Mappings of Attitude Analysis of Objects in Orbit. *Proceedings of the 6th European Conference on Space Debris, Darmstadt*, ESA Publications Division, European Space Agency, Noordwijk, The Netherlands.

5. S. Lemmens, H. Krag (2013). Sensitivity of automated Attitude Determination from ISAR Radar Mappings, *Proceedings of the Advanced Maui Optical and Space Surveillance Technologies Conference*, Maui Economic Development Board, http://www.amostech.com/.

6. F. Gini, M. Bardella , S. Casotto. (2014). Precise Non-Gravitational Forces modelling for GOCE, *Proceedings of the 24th Advances in the Astronautical Sciences Spaceflight Mechanics.* Vol. 152, ASS/AIAA.

7. F. Gini, M. Otten, T. Springer, et al. (2014). Precise Orbit Determination for the GOCE Re-entry Phase. *Proceedings of the fifth international GOCE user workshop*, ESA Publications Division, European Space Agency, Noordwijk, The Netherlands.

8. H. Klinkrad. (2006). Space Debris: Models and Risk Analysis. *Springer-Verlag*.

9. B. Bastida Virgili, S. Lemmens, T. Flohrer, et al. (2014). Influence of Solar Activity on Long Term Propagations. *Proceedings of the 65st International Astronautical Congress*.